

Evaluation of the effects of thermal variation and shrinkage of concrete in a building with cast-in-place concrete walls

L. B. Vargas¹ , A. Lübeck¹ , A. B. S. Santos Neto^{1*} 

*Contact author: almir.neto@ufsm.br

DOI: <https://doi.org/10.21041/ra.v13i1.591>

Received: 21/02/2022 | Received in revised form: 06/08/2022 | Accepted: 25/10/2022 | Published: 01/01/2023

ABSTRACT

The objective of this study was to evaluate the effects of thermal variations and shrinkage of concrete in a building with cast-in-place concrete walls. The walls and slabs of the building were modeled in SAP2000 commercial software with a Finite Element Method. The main tensile stresses in the walls and ceiling slab were verified against the serviceability limit state of fissure formation (SLS-F). Results showed that the effects of temperature variations and shrinkage from concrete drying developed main tensile stresses greater than the tensile strength of the concrete as prescribed by standard NBR 6118 (ABNT, 2014). Consequently, it was concluded that durability of the structure could be compromised by cracking from thermal and shrinkage loads.

Keywords: cast-in-place concrete walls; thermal variations; concrete shrinkage; numerical analysis, crack formation.

Cite as: Vargas, L. B., Lübeck, A., Santos Neto, A. B. S. (2023), “Evaluation of the effects of thermal variation and shrinkage of concrete in a building with cast-in-place concrete walls”, Revista ALCONPAT, 13 (1), pp. 112 – 130, DOI: <https://doi.org/10.21041/ra.v13i1.591>

¹ Programa de Posgrado en Estructuras y Construcción Civil – Universidade Federal de Santa Maria – RS, Brasil.

Contribution of each author

The author Vargas, L. B. developed the numerical model (100%), collected results and wrote the original manuscript (100%). Author Lübeck, A. proposed the topic (50%), revised the manuscript and improved numerical analysis discussion, results and conclusions (50%). Author Santos Neto, A. B. S. proposed the topic (50%), revised the manuscript and improved numerical analysis discussion, results and conclusions (50%).

Creative Commons License

Copyright 2022 by the authors. This work is an Open-Access article published under the terms and conditions of an International Creative Commons Attribution 4.0 International License ([CC BY 4.0](https://creativecommons.org/licenses/by/4.0/)).

Discussions and subsequent corrections to the publication

Any dispute, including the replies of the authors, will be published in the third issue of 2023 provided that the information is received before the closing of the second issue of 2023.

Evaluación de los efectos de las acciones térmicas y la retracción del hormigón en un edificio en paredes de hormigón moldeados *in Situ*

RESUMEN

Este estudio tiene como objetivo analizar los efectos de la variación térmica y la retracción por secado en un edificio con paredes de hormigón moldeados in situ. Las paredes y losas del edificio fueron discretizadas en el programa SAP2000 utilizando el Método de Elementos Finitos. Se analizaron los principales esfuerzos de tracción en las paredes y losa de cubierta, y se verificó el Estado Límite de Servicio de Formación de Grietas. Los resultados muestran que los efectos de la acción de la temperatura y la retracción por secado del hormigón desarrollan esfuerzos principales de tracción superiores a la resistencia a la tracción del hormigón prevista en la NBR 6118 (ABNT, 2014). Se encontró que las cargas térmicas y de retracción pueden resultar en el agrietamiento de las paredes y la losa del techo, cuando no se toman en cuenta.

Palabras clave: paredes de hormigón; efecto térmico; retracción del hormigón; análisis numérico, formación de grietas.

Avaliação dos efeitos das ações térmicas e de retração do concreto sobre uma edificação em paredes de concreto moldadas *in Loco*

RESUMO

Este trabalho tem como objetivo analisar os efeitos da variação térmica e da retração por secagem em um edifício de paredes de concreto moldadas in loco. As paredes e lajes da edificação foram discretizadas no programa SAP2000 por meio do Método dos Elementos Finitos. Foram analisadas as tensões principais de tração em quatro paredes e laje de cobertura, sendo verificado o Estado-Limite de Serviço de Formação de Fissuras. Os resultados mostram que os efeitos da ação da temperatura e principalmente da retração por secagem do concreto desenvolvem tensões principais de tração superiores a resistência à tração do concreto, prevista na NBR 6118 (ABNT, 2014). Assim, os carregamentos térmicos e de retração podem resultar na fissuração das paredes e laje de cobertura, colocando em risco a durabilidade da estrutura.

Palavras-chave: paredes de concreto; efeito térmico; retração do concreto; análise numérica, formação de fissuras.

Legal Information

Revista ALCONPAT is a quarterly publication by the Asociación Latinoamericana de Control de Calidad, Patología y Recuperación de la Construcción, Internacional, A.C., Km. 6 antigua carretera a Progreso, Mérida, Yucatán, 97310, Tel.5219997385893, alconpat.int@gmail.com, Website: www.alconpat.org

Reservation of rights for exclusive use No.04-2013-011717330300-203, and ISSN 2007-6835, both granted by the Instituto Nacional de Derecho de Autor. Responsible editor: Pedro Castro Borges, Ph.D. Responsible for the last update of this issue, Informatics Unit ALCONPAT, Elizabeth Sabido Maldonado.

The views of the authors do not necessarily reflect the position of the editor.

The total or partial reproduction of the contents and images of the publication is carried out in accordance with the COPE code and the CC BY 4.0 license of the Revista ALCONPAT.

1. INTRODUCTION

Cast-in-place concrete walls are widely used in Brazil and present advantages such as high productivity, rational use of materials and cost savings. Additionally, this procedure allows a higher quality control and substantially decreases wastage of building materials in construction yards. As such, it is considered an example of industrial technology applied to civil construction (Braguim, 2013).

A concrete wall system is defined in standard NBR 16055 (ABNT, 2012) as a self-supporting structural element, cast in-place, with a length 10x its thickness and able to carry loads along the same plane as the wall. All walls in a construction cycle of a building are cast in a single pouring stage with the reinforced slab interacting with the walls to form a monolithic structural element.

The recommended reinforcements for concrete walls are welded meshes to increase productivity and allow a more rational use of materials at the construction yard. Furthermore, rebars should be used to reinforce specific regions such as around openings, free edges, near holes, lintels or regions with high and localized stress.

One of the main concerns in concrete wall systems is crack formation (Wendler and Monge, 2018). This feature imparts safety concern in users and decreases structural durability due to the potential ingress of aggressive agents which can damage concrete and corrode reinforcements (Nakamura and Pinto, 2017). Several studies were conducted to identify the location and frequency of cracks in this type of construction system (Resende *et al.*, 2018; Lima *et al.*, 2020; Netto *et al.*, 2021; Padilha *et al.*, 2021). Results showed that the more susceptible regions for crack formation were edges of doors and windows, edges of walls, along the floor and foundation of large wall panels and on walls and ceiling slabs.

Thomaz and Carneiro (2013) pointed out that the driving mechanism for the appearance of cracks in concrete buildings were variations in temperature and shrinkage from drying. Unimpeded, these phenomena induced the expansion or contraction of concrete but, when constrained, created stresses that could exceed the tensile strength of concrete and induce crack formation (Micallef *et al.*, 2017).

Environmental factors affecting temperature are mostly ambient temperature, solar irradiation and radiative heat. Ambient temperature is the main factor affecting temperature of the entire structure and is represented by the uniform temperature variation (ΔT_u). On the other hand, solar irradiation and radiative heat are the main factors in the linear temperature gradient variation (ΔT_M). Exposure to sunlight heats up part of the building outer surface over a short period of time while the inside remains at a lower temperature (Larsson, 2009). The uniform temperature variation (ΔT_u) produces axial expansion or contraction in the case of heating or cooling, respectively, while the linear temperature gradient variation (ΔT_M) affects curvature. When these deformations are constrained, thermal-induced stresses develop (O'Brien *et al.*, 2015).

Shrinkage, on the other hand, is caused by water evaporation at the early stages of curing while concrete is still in a plastic phase and continues in the hardened phase (Rodrigues and Bauer, 2010). This process can be separated in several types such as carbonation, plastic, thermal, chemical, autogenous or drying (Markovski *et al.*, 2012). Drying shrinkage tends to be an aggressive process, especially in elements with exposed large surfaces (Recena, 2014). Specifically, shrinkage from

drying could be considered to have a similar effect as a uniform temperature variation (ΔT_u) as a constrained shrinking structural element also develops tensile stresses. Consequently, a temperature variation (ΔT) corresponding to a specific shrinkage deformation ($\epsilon_{cs}(t_\infty, t_0)$) could be determined and as a function of the thermal expansion coefficient of concrete (α) (Laranjeiras, 2017).

For the evaluation of cracks, standard NBR 6118 (ABNT, 2014) defined a serviceability limit state of fissure formation (SLS-F), which corresponded to a state in which acting stresses exceed tensile strength of concrete and cracks began to form. Following this procedure, this study presented an analysis of main tensile stresses on a structure composed of 4 walls and a ceiling slab corresponding to a building with cast-in-place concrete walls. The structure was subjected to different thermal loads, shrinkage from drying and permanent and variables loads. Regions of high stresses exceeding the tensile strength of concrete were identified for their potential in inducing crack formation in the structure.

2. METHODOLOGY

2.1 Building Model

The building model was a multi-apartment residential structure consisting of 3 floors. Each floor had an area of 210.06 m² and floorplan dimensions of 18.42 m x 13.82 m. Floor heights were of 2.70 m and the total height of the building was of 8.10 m. Building structure consisted of reinforced cast-in-place concrete walls 120 mm thick and solid reinforced concrete slabs 100 mm thick. As seen in Figure 1, each floor contained 4 apartments in a symmetrical arrangement and 4 walls were selected for analysis in this study. Walls 1 and 4 were external and consequently subjected to solar irradiation and linear temperature gradient variation (ΔT_M). Walls 2 and 3 were internal but part of Wall 2 was also exposed to solar irradiation. All walls had fame openings for windows and doors. The numerical model preserved the main geometrical characteristics of the building. However, measurements were adjusted to conform to multiples of 200 mm. Consequently, the numerical model did not contain variations larger than 300 mm and the results remained valid with respect to the original floorplan

2.2 Discretization of the structural model

Modeling and analysis were performed with SAP2000 V18 commercial software. All 3 floors of the building were modeled with a finite element model (FEM) so that the response of the entire structure was obtained from the interaction of all floor and wall elements in a linear-elastic analysis. In addition, SAP 2000 V18 also allowed the analysis of thermal and shrinkage effects on concrete. Structural elements in the numerical mesh were thin-shell quadrilateral elements measuring 200 mm x 200 mm. Thus, mesh nodes were perfectly superimposed along wall-wall intersections and wall-floor joints as well as openings for windows and doors. Thicknesses followed the structural elements with 120 mm walls and 100 mm slabs. Figure 2 presents a 3-D view of the building containing 49,169 thin-shell elements.

Boundary conditions were imposed on the nodes along the base of the building to prevent movement in any direction. Soil-structure interaction (SSI) effects were not considered since the

locked base nodes would induce elevated stresses in the building especially on walls directly connected to the foundation.

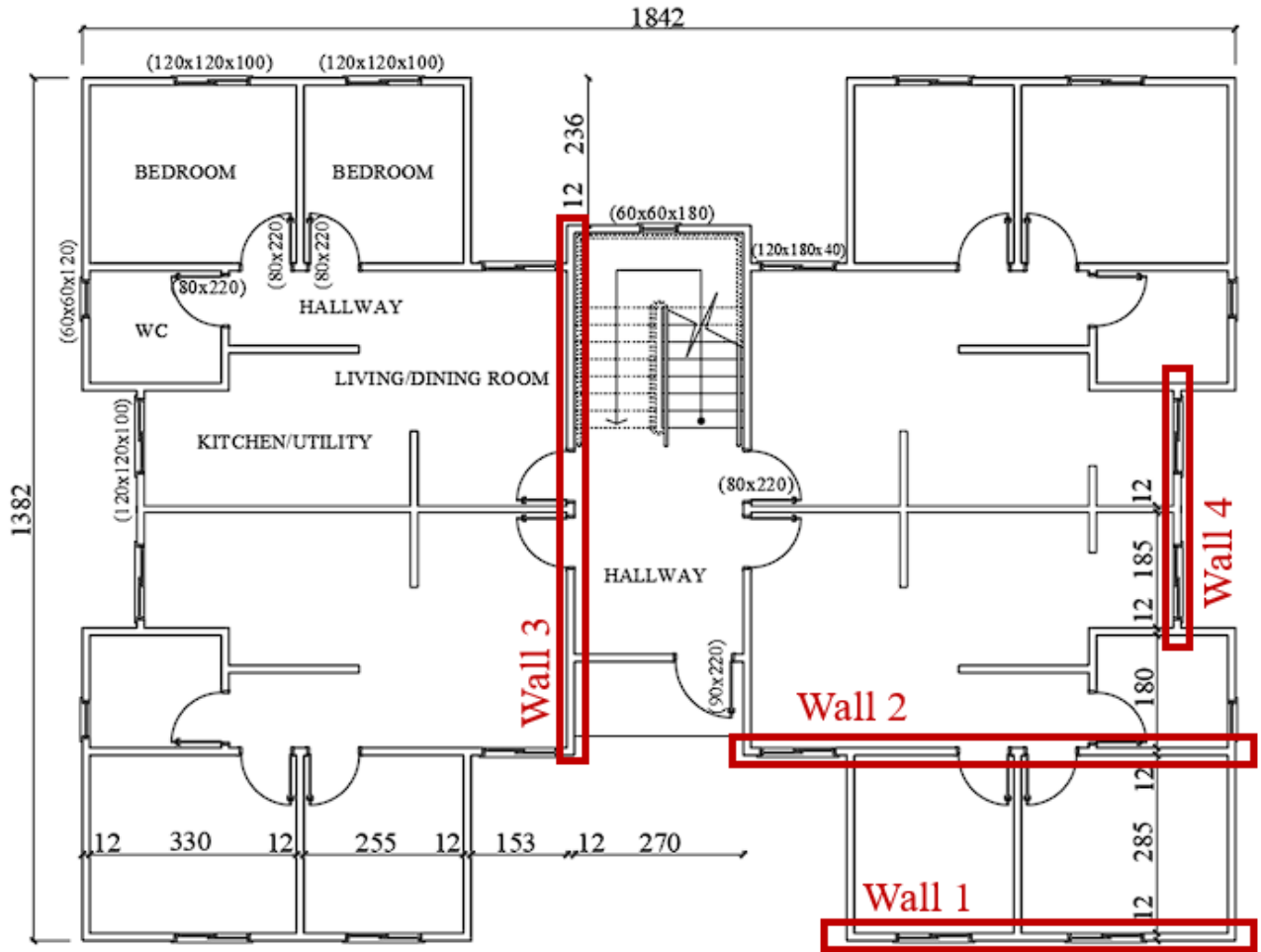


Figure 1. Residential building floorplan (cm).

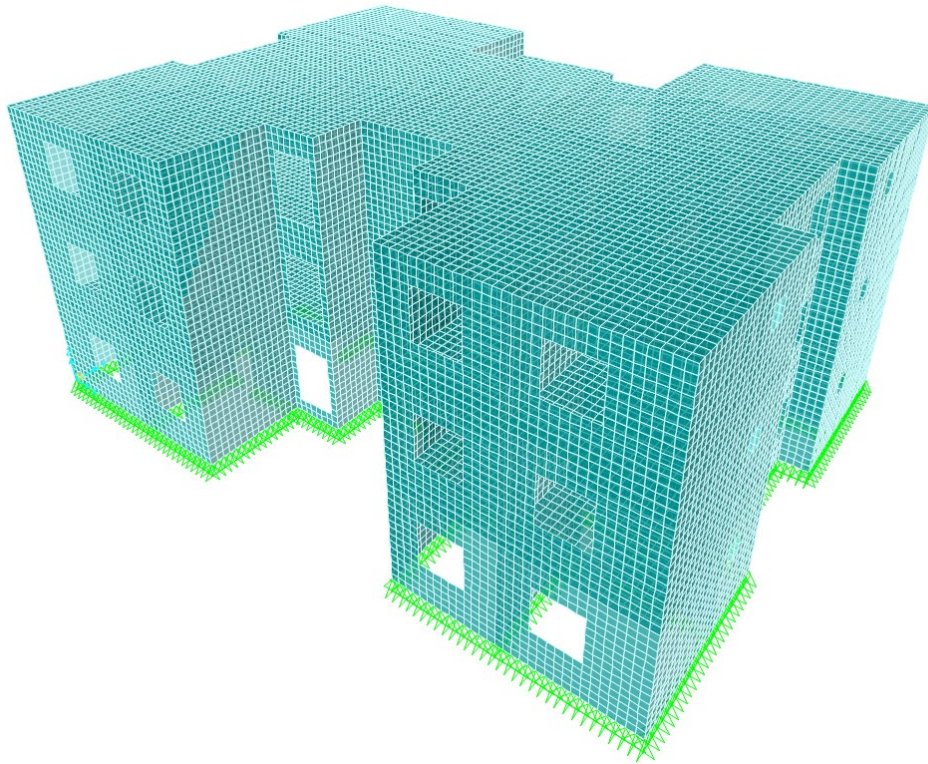


Figure 2. 3-D model of the building in SAP2000.

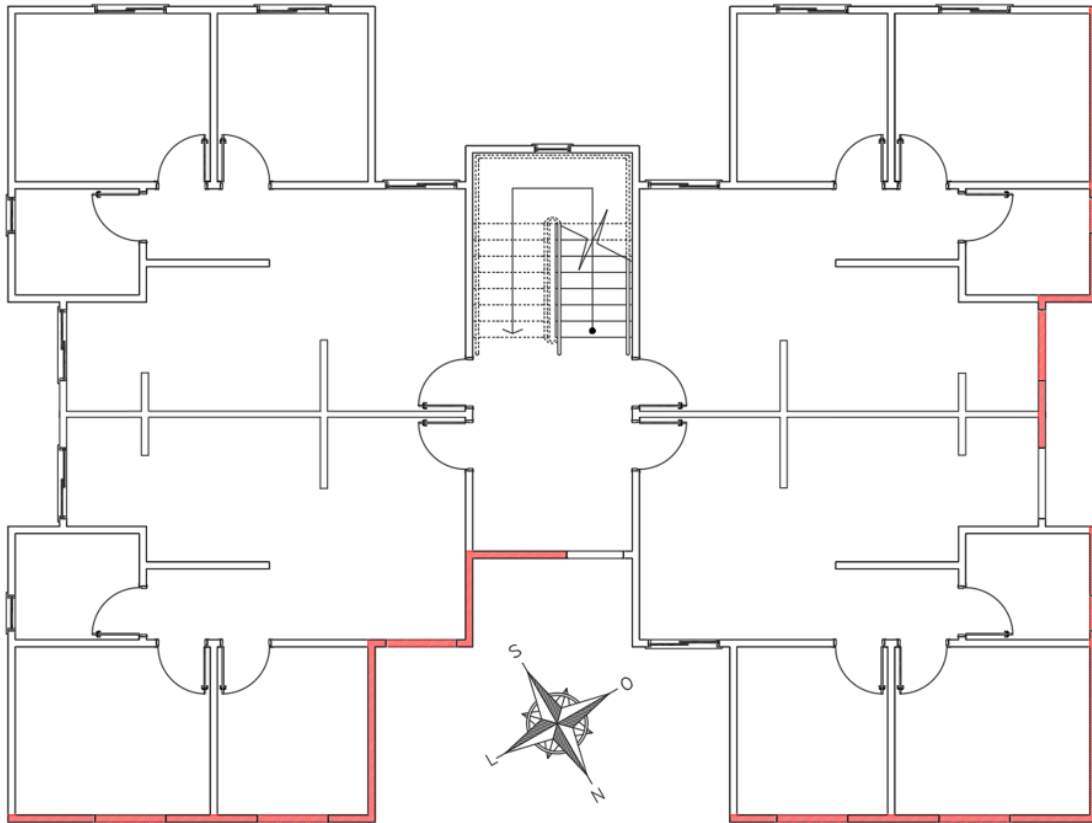


Figure 3. External walls subjected to solar irradiation (marked in red).

The effect of shrinkage from drying was determined from the thermal expansion coefficient of concrete, from which a temperature variation was obtained that would result in an equivalent specific contraction. Thus, shrinkage was modeled as a constant, negative thermal load along the thickness of an element (leading to contraction) present in all walls and slabs of the building.

2.4 Material Properties

Material properties of concrete were defined as prescribed in standard NBR 6118 (ABNT, 2014): characteristic compression strength (f_{ck}) of 30 MPa, specific weight of 25 kN/m³, dry modulus of elasticity of 27 GPa, Poisson coefficient of 0.20, thermal expansion coefficient of $1.0 \times 10^{-5} \text{ }^\circ\text{C}^{-1}$ and modulus of rigidity 12.92 GPa.

2.5 Loads and Combination of Loads

Permanent and variable loads were considered in accordance with standard NBR 6120 (ABNT, 2019). A typical floor was subjected to permanent loads of 1.0 kN/m² due to screed and floor and 0.25 kN/m² due to drywalls. Variable loads due to the use of the building were determined in accordance to occupancy: 3.0 kN/m² for common use areas, hallways and stairs, 2.0 kN/m² for utility and laundry rooms and 1.5 kN/m² for all remaining rooms. The ceiling slab had the same typical permanent loads but a variable load of 1.0 kN/m² since it would be only accessible for maintenance services.

No wind effects were considered since it would have impacted directly on wall stresses near the foundation, increasing or decreasing depending on wind direction. Since the focus of this study was on thermal and shrinkage stresses, compounding wind effects would preclude a precise evaluation of these factors.

Ambient temperatures followed the recommendations of Laranjeiras (2017). Regardless of the size of rooms, thermal loads consisted of uniform temperatures of +15 °C and -15 °C corresponding to summer and winter, respectively. A linear temperature gradient variation of 15 °C was added to the uniform temperature of walls subjected to solar irradiation so that its internal temperature would be +15 °C and the external temperature under sunlight would be +30 °C.

Shrinkage from drying was modeled as an effect of a uniform temperature variation. Following the guidelines of standard NBR 6118 (ABNT, 2014), an average ambient relative humidity of 75% typical of the state of Rio Grande do Sul, wall thickness of 200 mm and concrete age of 60 days, a specific deformation of -0.30% from shrinkage was determined, which corresponded to a uniform temperature variation of -30 °C. Shrinkage was considered a permanent and indirect action while temperature variations were considered indirect variable actions.

The serviceability limit state of fissure formation (SLS-F) analysis of the walls and ceiling slab were in accordance with NBR 6118 (ABNT, 2014) and made use of combinations of frequent service loads (FC) and rare service loads (RC). In order to isolate the higher tensile stresses developed by thermal loads, only combinations of rare loads (RC) were considered in this study. This decision was taken since thermal loads should only be taken as secondary variable loads with partial safety factor ψ_1 of 0.50 in RC, which was higher than the partial safety factor ψ_2 of 0.30 for FC.

This study made use of 6 rare load combinations (RC) as presented in Table 1. The first 4 combinations considered the dead load, permanent loads, variable loads, temperature variations and shrinkage. Shrinkage effects were also considered for all combinations except CR6. Although not suggested in standard NBR 6118 (ABNT, 2014), RC5 was setup with thermal variations as main variable loads while the remaining loads were deemed secondary. Finally RC6 considered only gravitational, permanent and accidental usage loads, in order to identify the behavior of the structure when not subjected to thermal or shrinkage loads. A similar analysis was conducted by Vargas (2021) in which dead loads, thermal and shrinkage loads were considered to evaluate the useful life of a building. As in this study, thermal and shrinkage loads were already accounted for during the construction phase.

The tensile strength of concrete ($f_{ctk,inf}$) for a class C30 concrete was given as 2.02 MPa in standard NBR 6118 (ABNT, 2014). Consequently, this value was taken as the limit for primary tensile stresses generated from the RCs in the evaluation of both walls and slabs which would indicate the initial formation of cracks.

Table 1. Load combinations used in this study.

Combination	Load composition (SLS – RC)
RC1	1.0 DL + 1.0 SR + 1.0 P + 1.0 Q
RC2	1.0 DL + 1.0 SR + 1.0 P + 1.0 Q + 0.5 UC
RC3	1.0 DL + 1.0 SR + 1.0 P + 1.0 Q + 0.5 UH
RC4	1.0 DL + 1.0 SR + 1.0 P + 1.0 Q + 0.5 (UH + LGH)
RC5	1.0 DL + 1.0 SR + 1.0 P + 1.0 (UH + LGH) + 0.4 Q
RC6	1.0 DL + 1.0 P + 1.0 Q

Legend: DL (Dead load), P (Permanent load), Q (Variable load), UH (Uniform Heating), UC (Uniform cooling), LGH (Linear gradient heating), SR (Shrinkage).

3. DISCUSSION AND ANALYSIS

The numerical analysis focused on main stresses on the 4 walls highlighted in Figure 1 and the ceiling slab. Tensile stress was limited to 2.02 MPa, which was the characteristic tensile strength of C30 concrete as defined in standard NBR 6118 (ABNT, 2014). In the contours of Figures 4 through 9, dark blue regions denoted regions in which this limit was exceeded.

Figure 4 shows main stresses for combination RC1 and Walls 1 and 2. Results showed that main stresses exceeded concrete strength on the first (ground) floor near the base of the walls. Stresses reached peak values in the order of 8.6 MPa and 6.0 MPa for Walls 1 and 2, respectively. This was the result of structural foundation elements restraining shrinkage deformations in the concrete and leading to higher stresses at the base when compared to higher floors. With respect to SLS-F, these regions would be considered prone to crack formation and would require higher steel reinforcement ratios. Crack formation from restrained shrinkage was also confirmed by Mikallef *et al.* (2017) and Gottsäter *et al.* (2019) which also recommended increased reinforcement in foundation elements. Figure 4 also showed localized stresses near the corners of openings and windows exceeding the strength limit with peaks of 6.9 MPa and 6.0 MPa for Walls 1 and 2, respectively. As per the recommendations of standard NBR 16055 (ABNT, 2012), further reinforcement would be needed around these openings to mitigate this effect. The lack of or improper complementary

reinforcements were shown by Padilha *et al.* (2021) and Lima *et al.* (2020) to allow cracks to appear starting from the corners of openings.

Another location affecting stress levels was the intersection of perpendicular walls. Such intersections restricted movement and, similar to foundation elements, produced higher tensile stresses. This effect was observable in two window openings of Wall 1 in Figure 4 where an intersection with an inner wall was present. Wall 2 presented higher stresses near windows, between doors and at the right side of the wall. Consequently regions with intersections and especially near openings must also have supplementary reinforcement to prevent cracks.

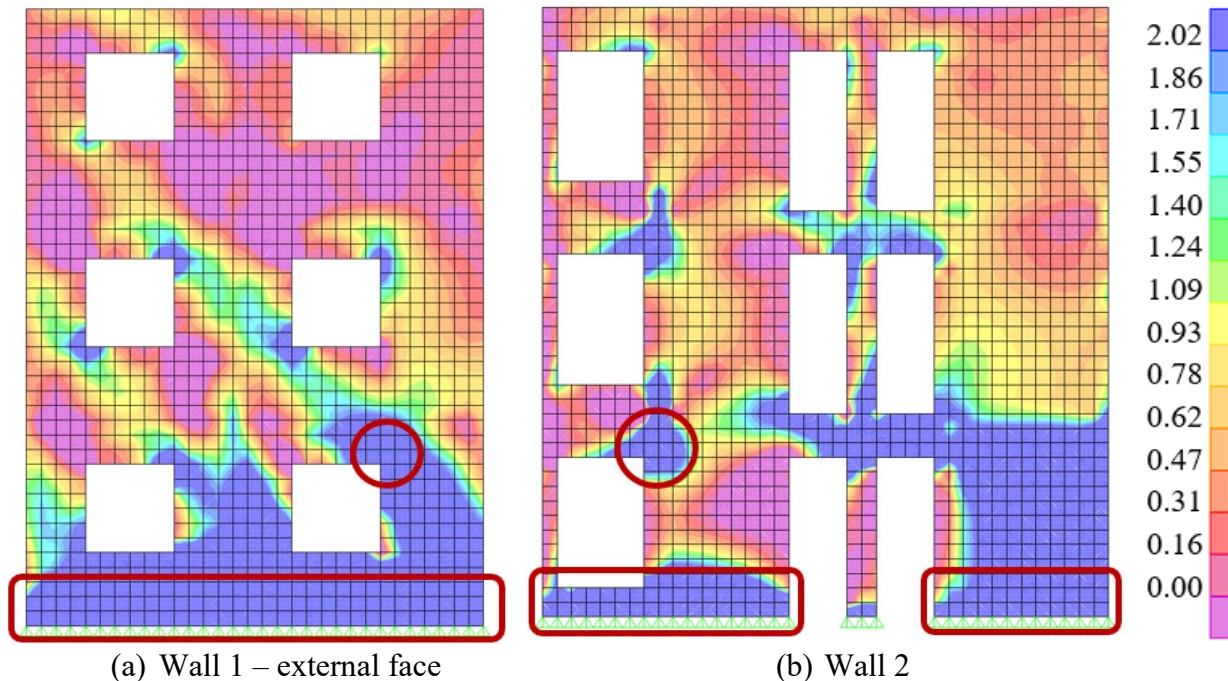
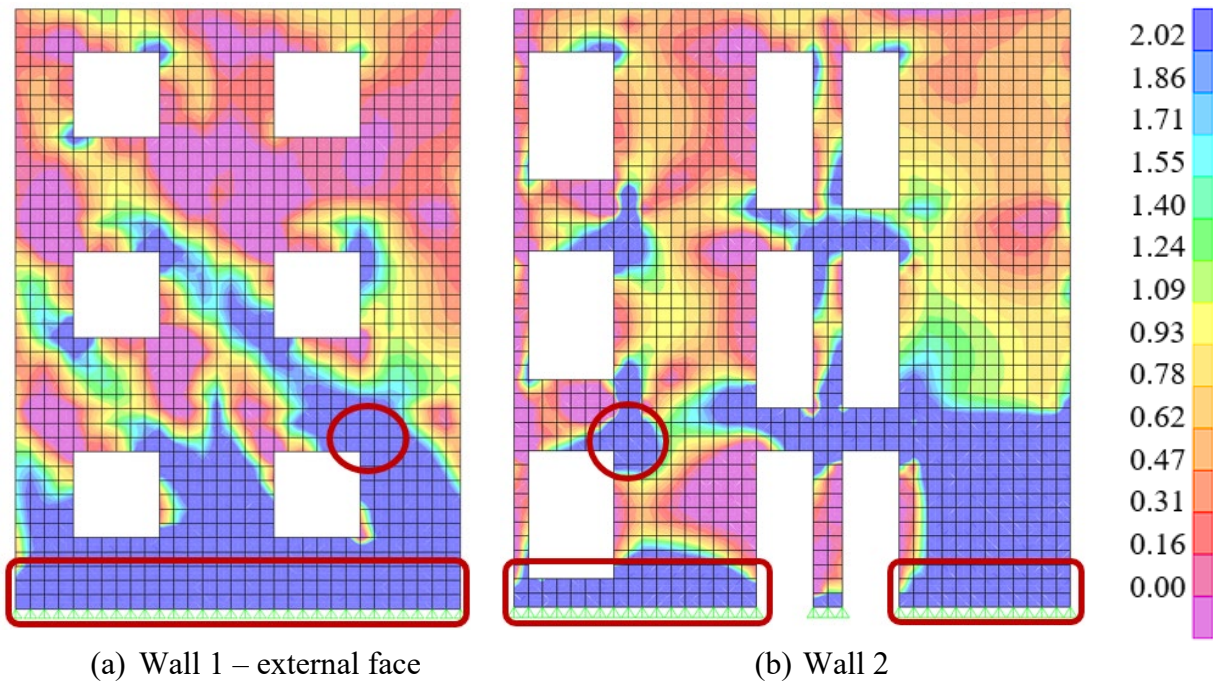


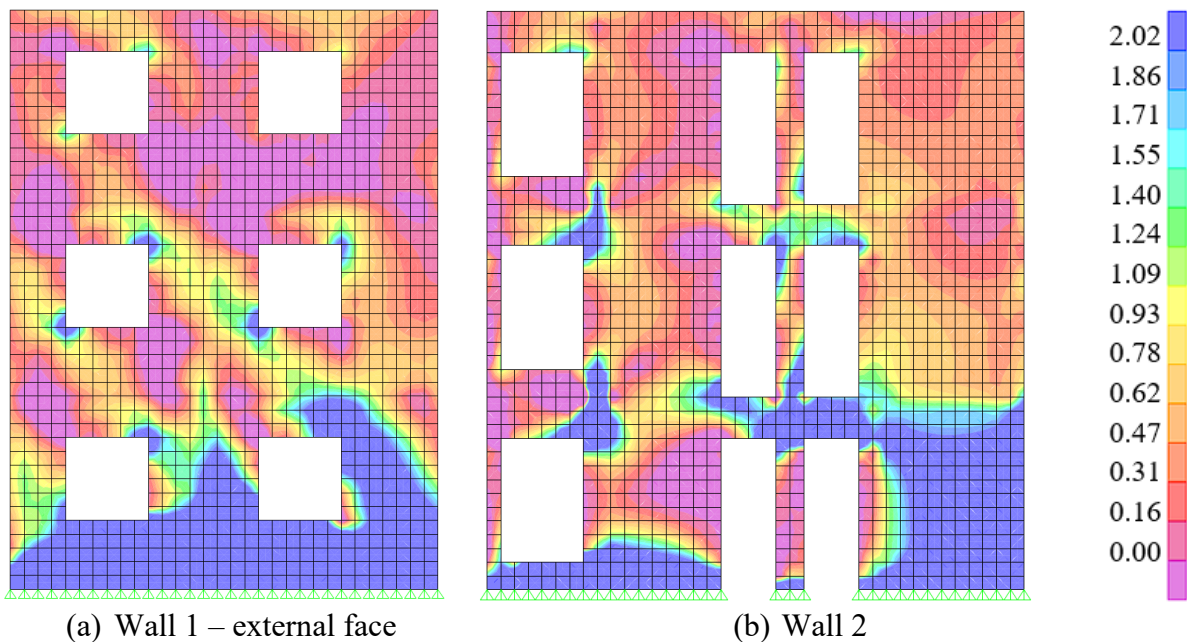
Figure 4. Main stress distribution for Walls 1 and 2 with combination RC1 (MPa).

Results for RC2 are shown in Figure 5 and are similar to RC1. As seen in Figure 5, RC2 main tensile stress regions followed the same pattern as RC1 but with higher peak values of 10.8 MPa and 8.0 MPa for the first floor and walls. Stresses near door and window openings peaked at 8.6 MPa and 8.0 MPa at Walls 1 and 2, respectively. The similarities and increase in main stresses were due to uniform cooling affecting the numerical model in a similar fashion as shrinkage, inducing a contraction in the structure.



(a) Wall 1 – external face (b) Wall 2
 Figure 5. Main stress distribution for Walls 1 and 2 with combination RC2 (MPa).

Stresses for combination RC3 are shown in Figure 6 and decreases in stress are observed in regions of high concentration. Thus, the highest stresses in Wall 1 were determined to be in the order of 6.4 MPa and 5.2 MPa for the base of the building and near window openings, respectively. The same corresponding decreases for Wall 2 were of 5.0 MPa and 6.0 MPa. This was the result of uniform heating opposing shrinkage by inducing an expansion in concrete. While lower than the stresses determined for RC1 and RC2, the values for RC3 were still above the strength limit of 2.02 MPa and consequently would still require complementary reinforcement to resist crack formation.



(a) Wall 1 – external face (b) Wall 2
 Figure 6. Main stress distribution for Walls 1 and 2 with combination RC3 (MPa).

Results for combination RC4 are shown in Figure 7 and denoted a general increase in stresses in both walls. Wall 1, under linear gradient thermal loading, presented new regions with main tensile stresses exceeding the limit of 2.02 MPa. These were at the intersection of a wall on the third floor with a stress of 2.1 MPa and the wall-floor and wall-ceiling slab joints on the third floor, with stresses of 2.1 MPa and 2.2 MPa, respectively. Thus, these new regions should also be marked to receive complementary reinforcement to prevent crack formation. The increase in main stresses in the third floor was also reported by Laranjeiras (2017) and El-Tayeb *et al.* (2019). Horizontal elements subjected to thermal loads expanded and consequently induced increased stresses in vertical elements. This was observed in Wall 2 which presented increases in stresses on the third floor albeit insufficient to result in crack formation

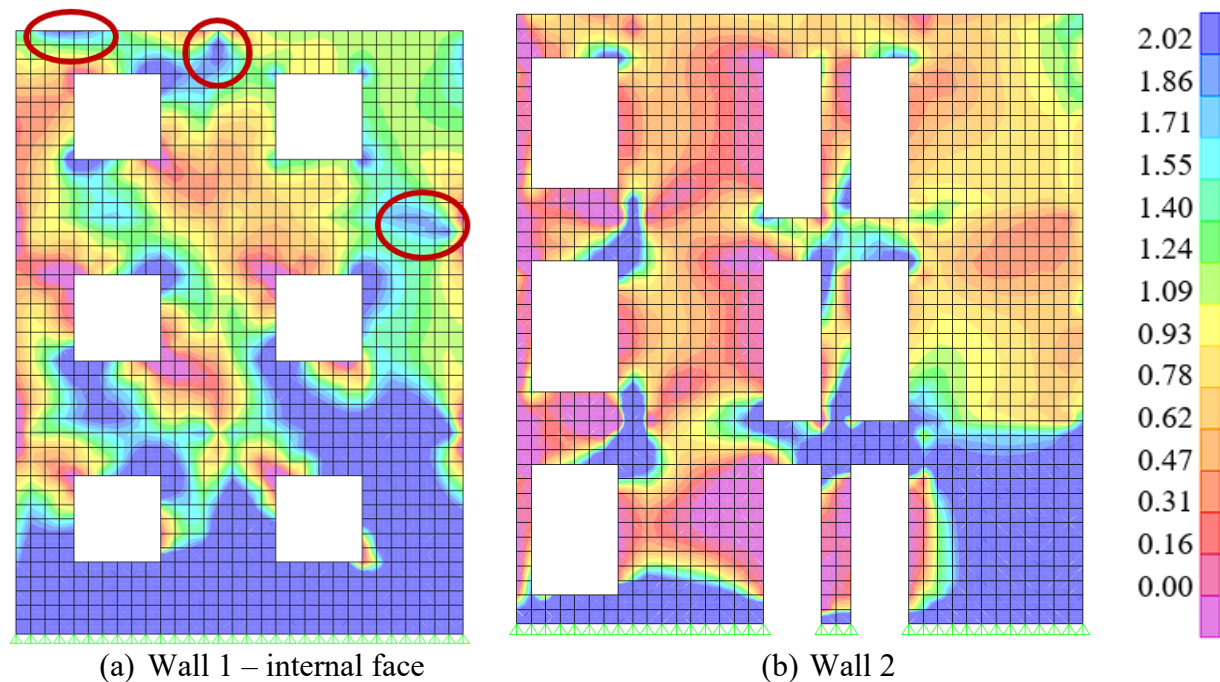
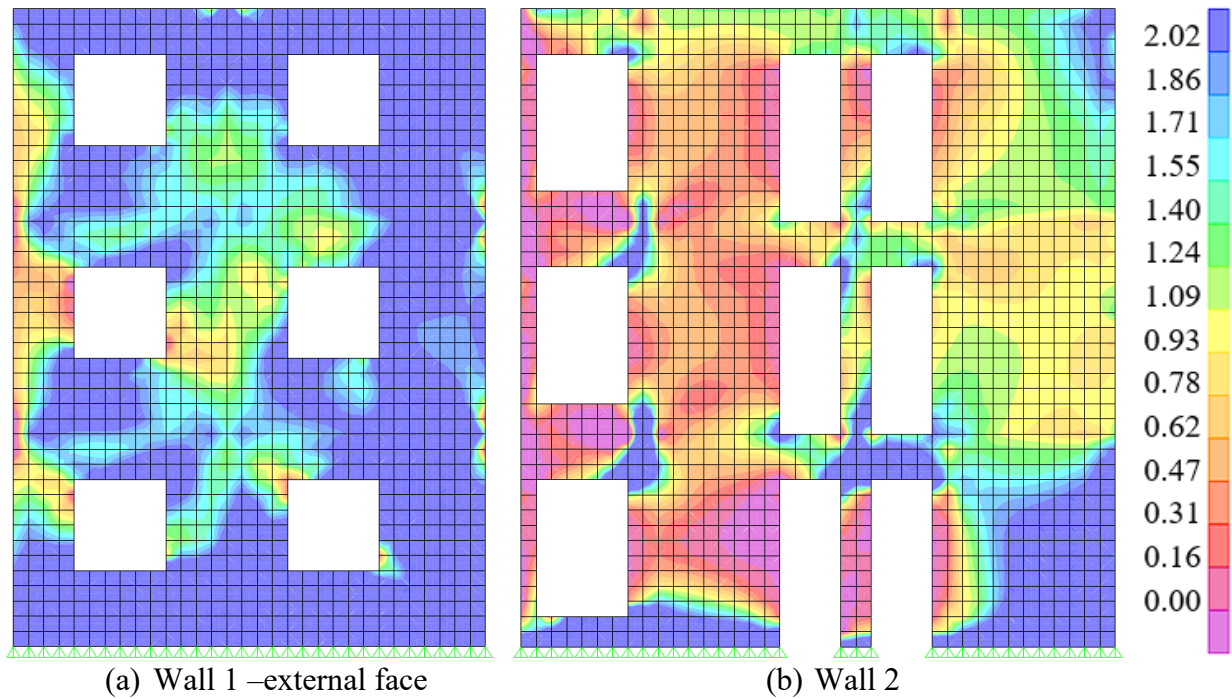


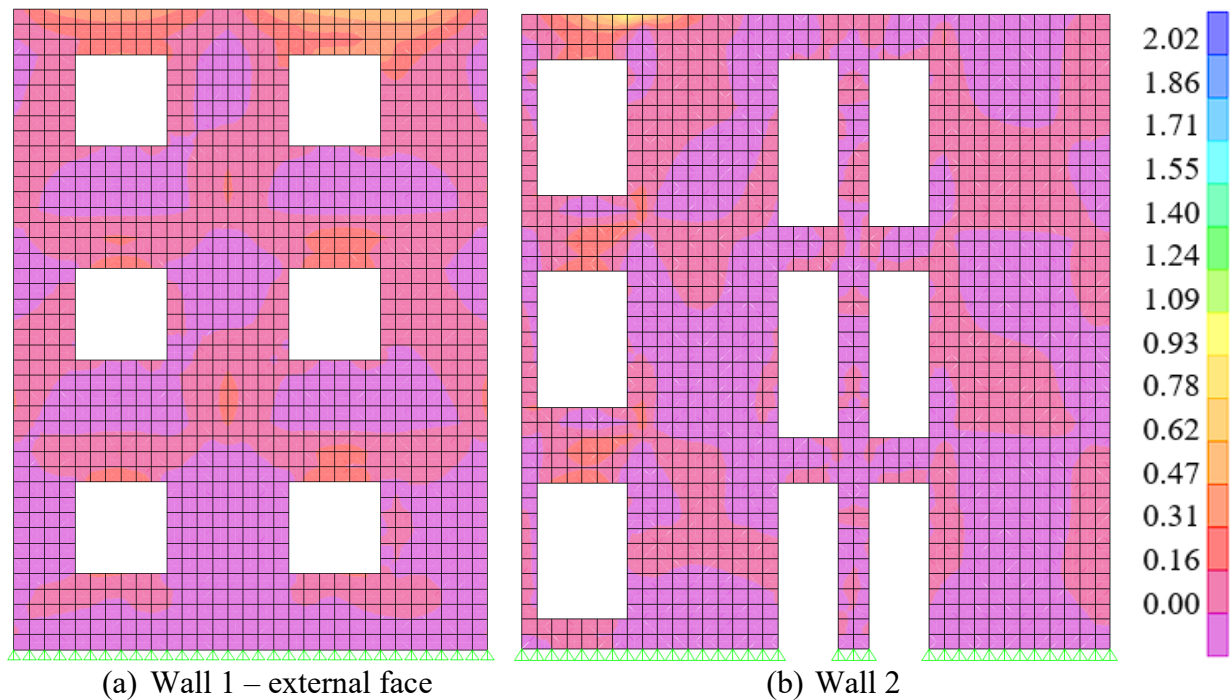
Figure 7. Main stress distribution for Walls 1 and 2 with combination RC4 (MPa).

Results for combination RC5, which was not part of standard NBR 6118 (ABNT, 2014), are shown in Figure 8. Overall the walls presented behaviors similar to RC4 with a slight increase in stresses in the main regions of interest. However, Wall 2 presented a new region near the ceiling slab with stresses exceeding the 2.02 MPa limit, which would result in crack formation.

Figure 9 presents results of combination RC6 for Walls 1 and 2. Regions near openings and the ceiling slab had main tensile stresses no higher than 0.93 MPa, much lower than the strength limit of 2.02 MPa. Additionally, regions near the foundation which presented stresses exceeding the strength limit now presented mostly compression. This result highlighted that considering only dead, permanent and variable loads were insufficient to predict regions of crack formation. Thus, a SLS-F analysis must include thermal loads and shrinkage effects.



(a) Wall 1 –external face (b) Wall 2
 Figure 8. Main stress distribution for Walls 1 and 2 with combination RC5 (MPa).



(a) Wall 1 – external face (b) Wall 2
 Figure 9. Main stress distribution for Walls 1 and 2 with combination RC6 (MPa).

The SLS-F analysis of Wall 3 and 4 for the combination of loads tested in this study are shown in Figures 10 and 11. Main stresses were shown at the foundation walls, corners of openings, wall intersections and ceiling slab joint, alongside a horizontal line denoting the 2.02 MPa limit strength. As seen in the figures, both walls were prone to crack formation except when thermal loads and shrinkage effects were not considered and must be reinforced accordingly.

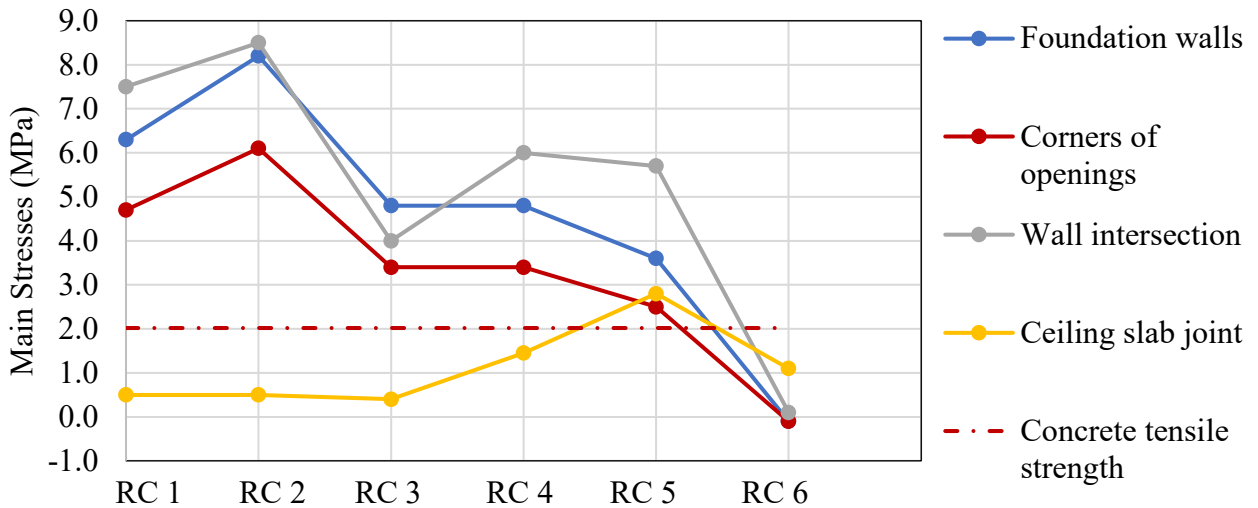


Figure 10. Peak main tensile stresses for Wall 3 (MPa).

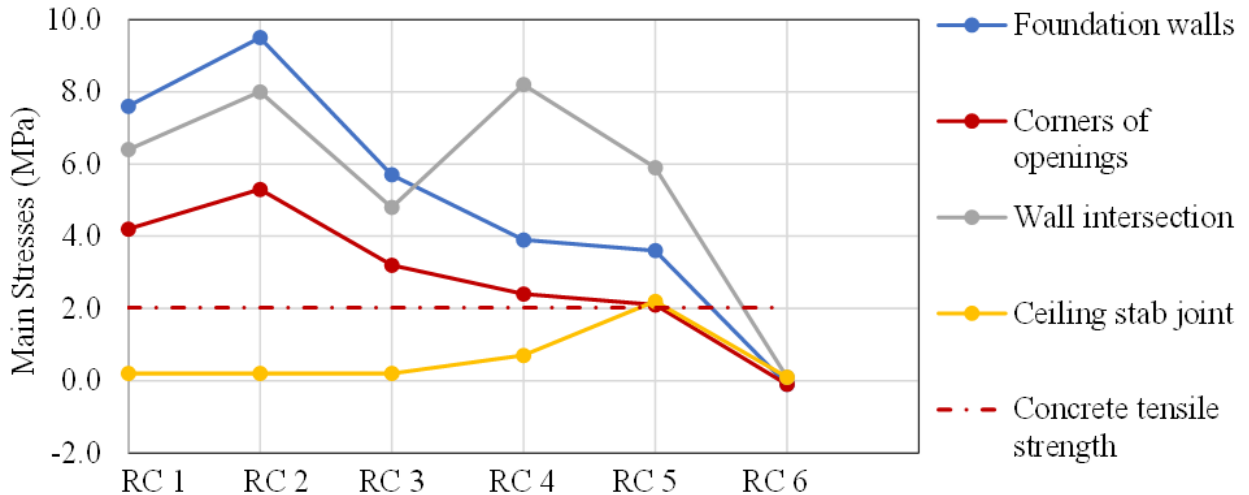


Figure 11. Peak main tensile stresses for Wall 4 (MPa).

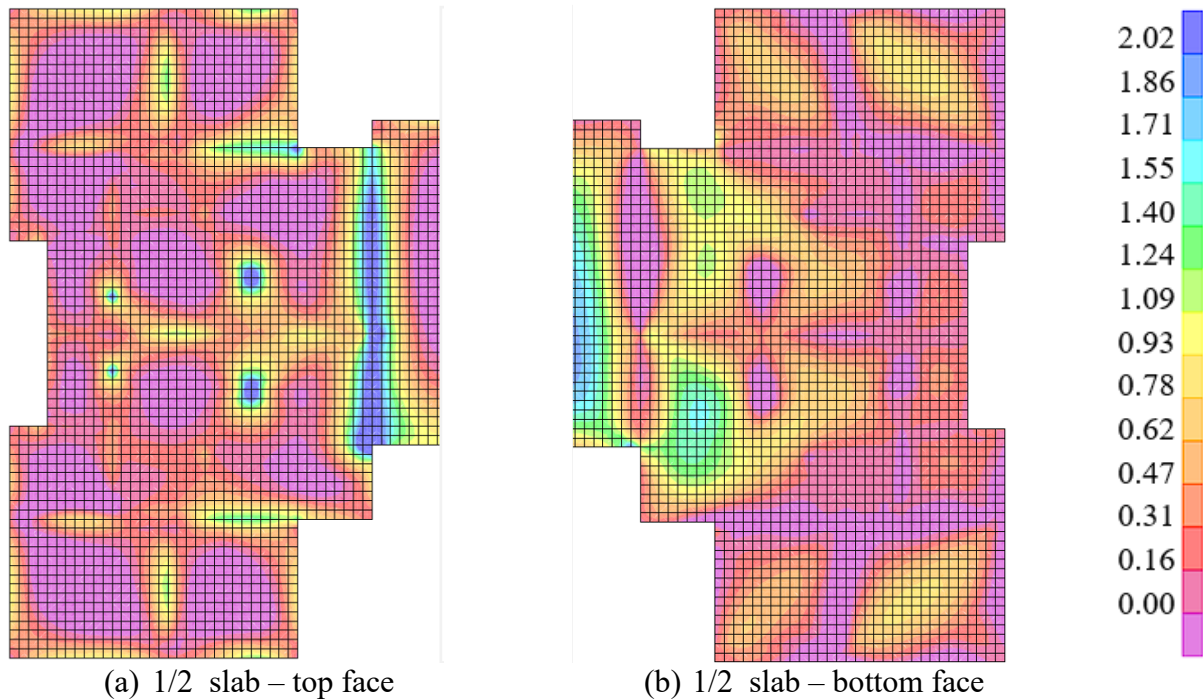
3.2 Ceiling slab analysis

Results for the top and bottom face of the ceiling slab are shown in Figures 12 to 16 for all combinations of loads of this study. Due to the bi-lateral symmetry of the structure, only half of the slab was presented. As determined in the previous subsection, walls subjected to uniform temperature variations with no solar irradiation had decreased main tensile stresses. Consequently, no ceiling slab analysis was conducted for combination RC3.

Figure 12 shows that main stresses of approximately 2.5 MPa develop in excess of the SLS-F limit for combination RC1. The affected region was where the slab narrowed and joined Wall 3. Thus, the stresses were due to a combination of the reduction in area of the slab, Wall 3 restricting deformations from shrinkage and the natural behavior of the structure stressing the top face of the ceiling slab due to the support provided from the wall.

Thus, in order to prevent crack formation, top reinforcement of the ceiling slab must be calculated to resist the increased stress and the steel reinforcement ratio adjusted accordingly. Alternatively,

stresses exceeding the 2.02 MPa limit and crack formation might be avoided with placement of expansion joints in narrowing regions.

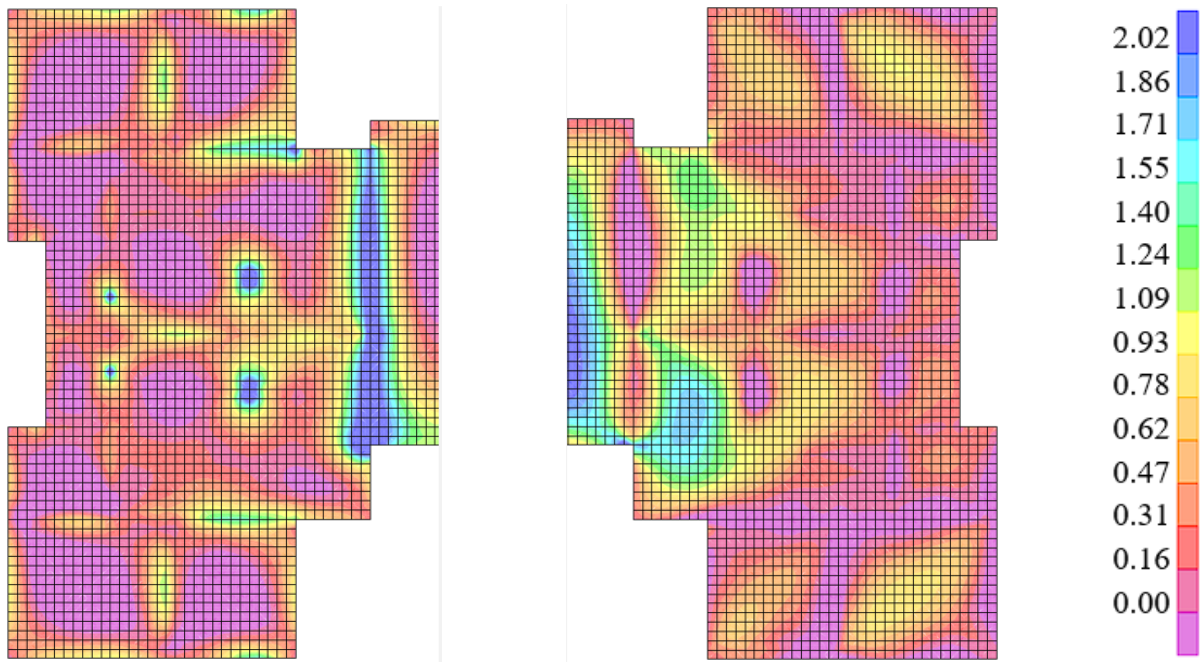


(a) 1/2 slab – top face
 (b) 1/2 slab – bottom face
 Figure 12. Main stresses in the ceiling slab for combination RC1 (MPa)

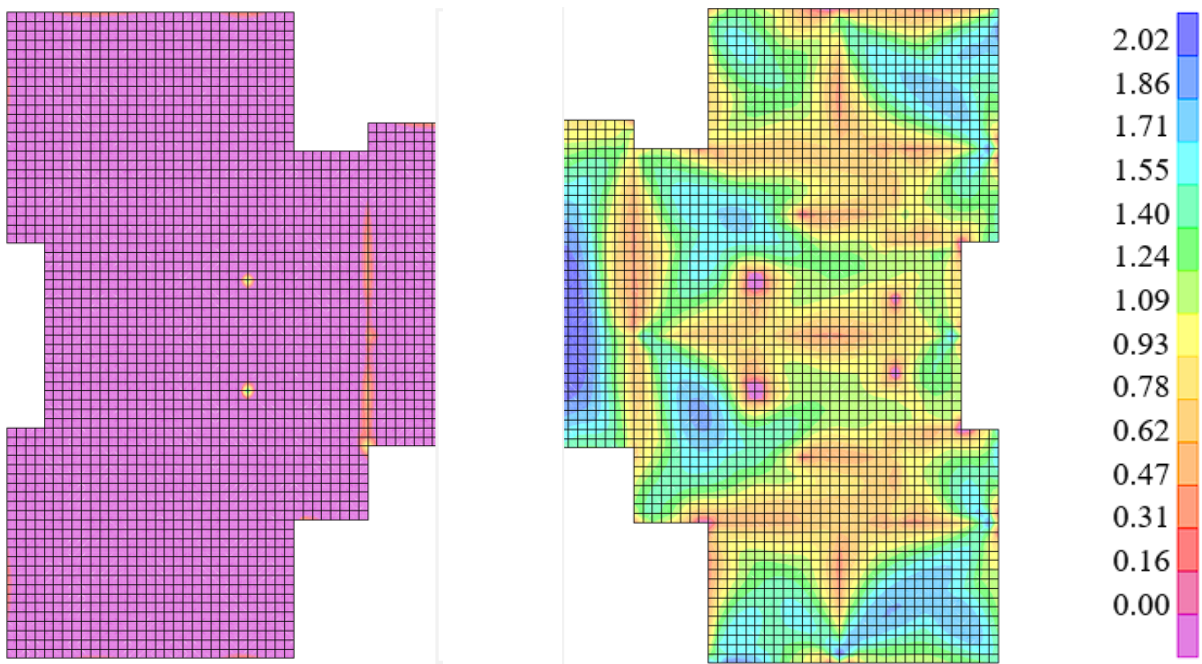
For the uniform cooling of combination RC2, Figure 13 shows an increase in the critical crack formation region on the top face of the ceiling slab, with tensile stresses in the order of 3.5 MPa. Additionally, the bottom face of the slab also presented stresses of approximately 2.10 MPa, in excess of the strength limit.

Figure 14 shows results for the linear gradient heating of combination RC4 due to solar irradiation. The top face of the ceiling slab was mostly under compressive stresses while the bottom face had increased main tensile stresses of up to 2.10 MPa at the center. This denoted the need to adequately design bottom reinforcement to prevent crack formation.

Figure 15 shows results for the non-standardized combination RC5 in which thermal loads were considered the main variable loads. In this case, the bottom face presented stresses exceeding the limit of crack formation on most of its area. Consequently, like RC4, bottom reinforcement must be designed accordingly to deal with the most aggravating regions.

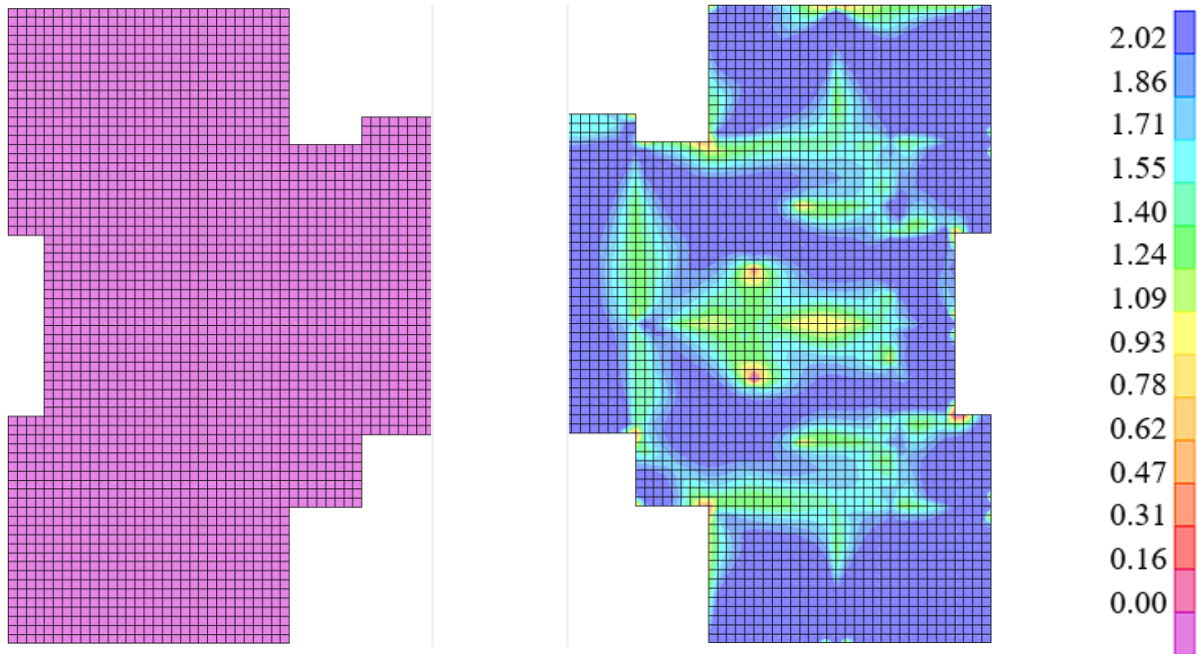


(a) 1/2 slab – top face (b) 1/2 slab – bottom face
 Figure 13. Main stresses in the ceiling slab for combination RC2 (MPa)



(a) 1/2 slab – top face (b) 1/2 slab – bottom face
 Figure 14. Main stresses in the ceiling slab for combination RC4 (MPa)

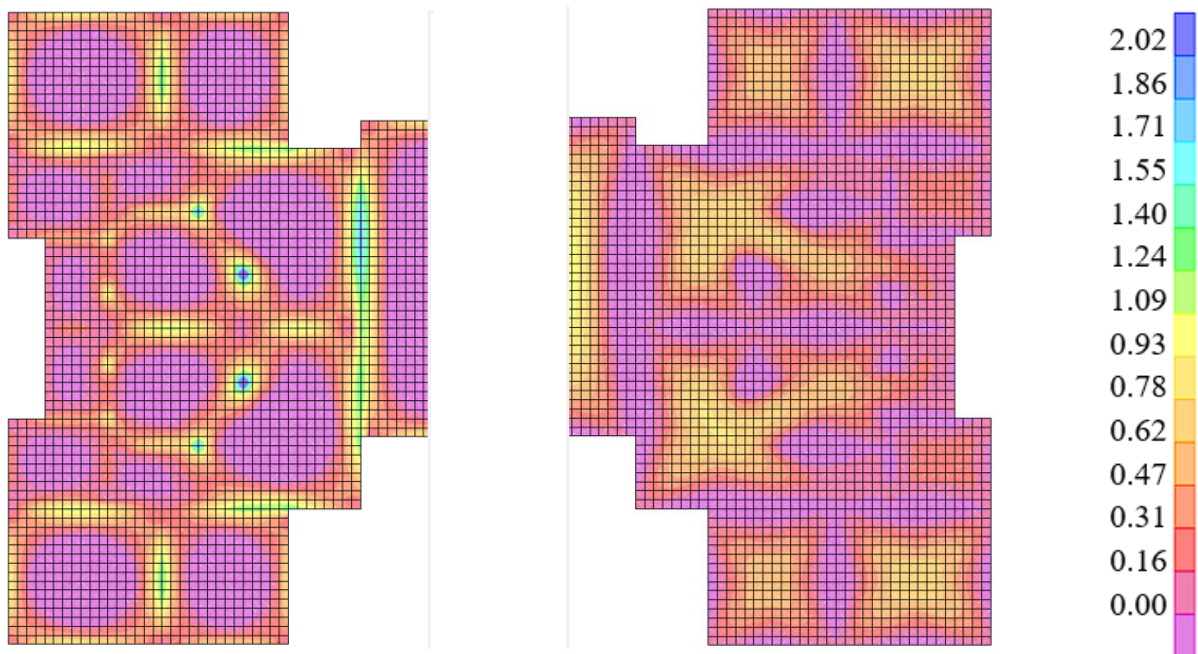
Figure 16 shows the results of combination RC6, which did not include thermal loads or shrinkage effects. Main tensile stresses developed on the top face at the wall-slab joints while the bottom face presented a central stress region. For this combination, no regions of crack formation were identified from the application of gravitational loads only.



(a) 1/2 slab – top face

(b) 1/2 slab – bottom face

Figure 15. Main stresses in the ceiling slab for combination RC5 (MPa)



(a) 1/2 slab – top face

(b) 1/2 slab – bottom face

Figure 16. Main stresses in the ceiling slab for combination RC6 (MPa)

4. CONCLUSIONS

This study determined that thermal loading and shrinkage effects could induce tensile stresses in excess of the 2.02 MPa limit prescribed NBR 6118 (ABNT, 2014) for C30-class concrete in cast-in-place walls.

Combinations considering only shrinkage (RC1) or shrinkage with uniform cooling (RC2) presented the highest tensile stresses of all cases tested in this study. Consequently, these combinations were deemed the most adequate to allow the identification of regions of crack formation in walls and ceiling slabs.

A full building model approach was justified since restrictions on expansion and contraction on walls, slabs and foundation significantly affected the resulting stresses. Regions near foundation elements and wall intersections had the highest tensile stresses under uniform cooling and shrinkage.

Uniform temperature variations were only significant when combined with variable linear temperature gradients. This yielded stresses in excess of the strength limit especially in the joint between walls and ceiling slab.

Consequently, to ensure structural durability under SLS-F, thermal loads and shrinkage effects must be considered. It should be highlighted that applying only the usual gravitational loads for analysis were insufficient to identify regions of potential crack formation.

Future studies should consider the following factors: a) adding wind effects alongside uniform cooling and shrinkage effects; b) include flexible foundations in the soil-structure interface to improve structural interaction with foundation elements and c) design walls and ceiling slabs with usual loads and thermal loads and shrinkage to compare the required increase in steel reinforcement ratio.

5. REFERENCES

- Associação Brasileira de Normas Técnicas. (2019). *NBR 6120: Ações para o Cálculo de Estruturas de Edificações*. Rio de Janeiro.
- Associação Brasileira de Normas Técnicas. (2012). *NBR 16055: Parede de Concreto Moldada no Local para a Construção de Edificação: Requisitos e Procedimentos*. Rio de Janeiro.
- Associação Brasileira de Normas Técnicas. (2014). *NBR 6118: Projeto e Execução de Obras de Concreto Armado*. Rio de Janeiro.
- Braguim, T. C. (2013), “*Utilização de modelos de cálculo para projeto de edifícios de paredes de concreto moldadas no local*”. Disertación de Maestría, Escola Politécnica, Universidade de São Paulo, São Paulo, DOI: <https://doi.org/10.11606/D.3.2013.tde-18082014-144751>
- Computers & Structures Inc. (2016), *CSI Analysis Reference Manual for SAP2000*. Berkeley, California, USA.
- El-Tayeb, Essam H.; El-Metwally, Salah E.; Askar, Hamed S.; Yousef, Ahmed M. (2017), *Thermal analysis of reinforced concrete beams and frames*. HBRC Journal, 13:1, 8-24, DOI: <https://doi.org/10.1016/j.hbrcj.2015.02.001>

- Gottsäter E., Johansson M., Plos M., Ivanov O. L. (2019), *Crack widths in base restrained walls subjected to restraint loading*. Engineering Structures, Volume 189, Pages 272-285, ISSN 0141-0296, DOI: <https://doi.org/10.1016/j.engstruct.2019.03.089>
- Laranjeiras, A. C. R. (2017), “*Edifício sem juntas*”. Salvador, Brasil. 46 p.
- Larsson, O. (2009), *Modelling of temperature profiles in a concrete slab under climatic exposure*. Structural Concrete. v. 10, n. 4, p. 193-201, ISSN 1464-4177, DOI: <https://doi.org/10.1680/stco.2009.10.4.193>
- Lima, K. B. A.; Borba, F. V.; Rocha, J. P.; Paixão, M. A. S.; Araújo, W. M. P.; Viana, S. W. J. P.; Nunes, L., L., L. (2020), *Fissuras em paredes de concreto em um conjunto residencial, localizado em São José de Ribamar – Maranhão*. Revista Científica Multidisciplinar Núcleo do Conhecimento. Ano 05, Ed. 04, Vol. 05, pp. 148-163. Abril de 2020. ISSN: 2448-0959. Disponível em: <https://www.nucleodoconhecimento.com.br/engenharia-civil/fissuras-em-paredes>
- Markovski, G., Čeček, M., Šahinagić-Isović, M. (2012), *Shrinkage strain of concrete - causes and types*. GRAĐEVINAR, 64, 9, DOI: <https://doi.org/10.14256/JCE.719.2012>
- Micallef M., Vollum R. L., Izzuddin B. A. (2017), *Crack development in transverse loaded base-restrained reinforced concrete walls*. Engineering Structures, Volume 143, 2017, Pages 522-539, ISSN 0141-0296, DOI: <https://doi.org/10.1016/j.engstruct.2017.04.035>.
- Nakamura, J.; Pinto, J. R. *Fissuras põem em risco a vida útil das estruturas de concreto*. Portal AECweb. [S.I.] 2017. Disponível em: <https://www.aecweb.com.br/revista/materias/fissuras-poem-em-risco-a-vida-util-das-estruturas-de-concreto/16243>. Acesso em: 24 de abr. 2021.
- Netto, L. G. R.; Souza, V. V.; Farias, B. M. (2021), *Análise das Manifestações Patológicas no Pós-Obra do Método Construtivo de Paredes de Concreto em Edifícios de Habitações Populares na Cidade do Rio de Janeiro*. Epitaya E-books, [S. l.], v. 1, n. 6, p. 368-397, DOI: <https://doi.org/10.47879/ed.ep.2021250p368>. Disponível em: <https://portal.epitaya.com.br/index.php/ebooks/article/view/184>. Acesso em: 5 jul. 2022.
- O'Brien, E. J., Keogh, D. L.; O'Conner, A. J. (2015), “*Bridge deck analysis*”. 2 ed. Boca Raton: CRC Press. cap. 2, p. 46-55.
- Padilha, F.; Carneiro, L. R. S.; Poggiali, F. S. J. (2021), “*Análise de manifestações patológicas em sistemas de paredes de concreto moldadas in loco*”. XVI Congresso Latino-Americano de Patología de Construcción y XVIII de Control de Calidad en la Construcción. ISBN: 978-65-86819-19-9, DOI: <https://doi.org/10.4322/conpat2021.461>
- Recena, F. P. (2014), “*Retração do concreto*”. Porto Alegre: EDIPUCRS, 151 p.
- Resende, P. B., Martins, R. J. F., Freitas, M. S. (2018), “*Fissuras causadas por movimentações térmicas no concreto*”. Semana Nacional de Ciência e Tecnologia, p. 1-10.
- Rodrigues, G. S. S.; Bauer, E. (2010), “*Avaliação da retração por secagem a baixas idades em concretos estruturais na região da grande goiânia*”. In: 52º Congresso Brasileiro do Concreto, Fortaleza. 52. Congresso Brasileiro do Concreto. São Paulo, 2010. v. 52. p. 1-14. Disponível em: <http://materialsandmateriais.blogspot.com/2013/08/artigo-tecnico-at-08-retracao-do.html>
- Thomaz, E., Carneiro, L. A. V. (2013), “*Manifestações patológicas na construção: alguns casos reais de fissuração em paredes de edifícios de concreto armado*”. in: IX International Congress on Pathology and Repair of Structures, João Pessoa (Brasil), 16 p.

Vargas, L. B. (2021), *Avaliação das Ações Térmicas e de Retração em uma Edificação em Paredes de Concreto Moldadas in Loco*. Trabajo de Conclusión de la carrera en Ingeniería Civil, Universidade Federal de Santa Maria. 78p.

Wendler, A., Monge, R. (2018), “*Paredes de concreto – como ter uma obra sem manifestações patológicas*”. *Concreto e Construções*, São Paulo, Ano XLVI, Ed. 90, p. 38-41, abr./jun. 2018.

ISSN: 1809-7197. Disponível em:

http://ibracon.org.br/Site_revista/Concreto_Construcoes/ebook/edicao90/files/assets/basic-html/page38.html. Acesso em: 20 jul. 2022.